RESEARCH ARTICLE | MARCH 23 2026

# *In situ* frequency tuning of superconducting resonators via nonlinear kinetic inductance

M. R. Vissers ; J. D Wheeler ; P. Szypryt ; A. Giachero ; J. E. Austermann ; J. Hubmayr ; G. C. O'Neil ; J. N. Ullom ; J. Gao



*Appl. Phys. Lett.* 128, 122601 (2026)
https://doi.org/10.1063/5.0316371

Applied Physics Letters ARTICLE pubs.aip.org/aip/apl

# *In situ* frequency tuning of superconducting resonators via nonlinear kinetic inductance

Cite as: Appl. Phys. Lett. **128**, 122601 (2026); doi: 10.1063/5.0316371
Submitted: 12 December 2025 · Accepted: 26 February 2026 ·
Published Online: 23 March 2026

View Online Export Citation CrossMark

M. R. Vissers,[1,a)] J. D Wheeler,[1] P. Szypryt,[1,2] A. Giachero,[1,2,3] J. E. Austermann,[1] J. Hubmayr,[1] G. C. O'Neil,[1] J. N. Ullom,[1] and J. Gao[1,2]

## AFFILIATIONS

[1]Quantum Sensors Division, National Institute of Standards and Technology, Boulder, Colorado 80305, USA
[2]Department of Physics, University of Colorado, Boulder, Colorado 80309, USA
[3]Department of Physics, University of Milano-Bicocca, Milan 20126, Italy

[a)]Author to whom correspondence should be addressed: michael.vissers@nist.gov

## ABSTRACT

Superconducting microresonators have diverse applications, including microwave kinetic inductance detectors, microwave superconducting quantum interference device multiplexers, and superconducting qubits. Arrays of such devices are typically addressed using microwave frequency combs with probe tones matched to individual device resonances. However, resonator frequency collisions caused by wafer non-uniformity and fabrication variations significantly limit usable device yields. In this Letter, we present a technique that mitigates these frequency collisions without the need for *ex post facto* processing. By leveraging nonlinear kinetic inductance and persistent current in a superconducting loop, we achieve *in situ* tuning of individual resonator frequencies within an array during device cooldown, effectively resolving frequency collisions in a way that is both highly flexible and reversible. We successfully demonstrate this technique by tuning a small array of four resonators to both identical frequencies and a uniformly spaced frequency comb. This *in situ* resonator tuning approach provides a universal solution for improving yield and multiplexing density in large resonator arrays, addressing a critical need for scaling up superconducting detector and qubit systems.





Superconducting microwave resonators have found broad usage in different applications such as superconducting qubits,[1,2] kinetic inductance detectors (KIDs),[3] and microwave superconducting quantum interference device (SQUID) multiplexers.[4] The inherent frequency multiplexability of the resonator is an advantage that enables multiple resonators to be addressed and read out through a shared microwave transmission line. However, multiplexing is only successful if the resonators are sufficiently separated in the frequency domain. Otherwise, frequency collisions occur, rendering the affected resonators inoperable, compromising device performance, or increasing crosstalk between readout channels. Frequency collisions can arise from various factors, including wafer non-uniformity and fabrication spatial variations. For example, local inhomogeneities and nonlocal gradients in film thickness or critical temperature ($T_c$) result in kinetic inductance variations, which consequently lead to spatial variations in resonant frequency. As resonator array sizes continue to expand, exemplified by large-scale KID arrays[5,6] containing thousands of resonators, and as readout system costs drive applications to higher multiplexing factors,[7] the importance of accurate frequency placement becomes increasingly critical. Additionally, more stringent crosstalk requirements in quantum computing applications further emphasize the need for precise frequency control.

To address this critical issue, we previously developed wafer mapping and post-measurement correction techniques.[8,9] By using a light-emitting diode (LED) array to illuminate individual resonators, the wafer mapping technique allows us to establish a direct correlation between each resonator's physical position on the wafer and its resonant frequency. In the post-measurement correction procedure, resonant frequency collisions are corrected by returning the array to the cleanroom, where it is re-patterned and re-etched to modify the resonant frequency of some or all of the resonators. While this procedure has demonstrated the ability to greatly improve frequency placement and recover collided resonators, it is time-consuming, limited by lithographic precision, and risks wafer damage. Conversely in this work, we present the development of an improved procedure to tune the resonances *in situ* and, importantly, lock the tuned resonances in place using a superconducting

persistent current. This approach eliminates the need for multiple fabrication cycles while maintaining precise frequency control, opening the door to even higher effective multiplexing factors.

Our new resonator frequency tuning scheme leverages the inherent nonlinear kinetic inductance of superconducting films.[10] Unlike conventional superconductors such as Nb and Al, high-resistivity superconductors including TiN and NbTiN exhibit substantial kinetic inductance that varies with current, $I$, according to Ref. 11

$$L_k(I) = L_k(0)\left[1 + (I/I_*)^2 + O(I^4)\right], \quad (1)$$

where $L_k(0)$ represents the kinetic inductance at zero current and $I_*$ is a characteristic current on the order of the critical current $I_c$ that sets the magnitude of the nonlinearity. Due to its quadratic dependence on current, the nonlinear kinetic inductance of a superconductor behaves analogously to Kerr media in nonlinear optics. This phenomenon has been exploited to create several novel devices, including parametric amplifiers,[12–14] frequency converters,[15,16] and current sensors.[17–19] Studies have been made of the dependence of the nonlinear kinetic inductance on bias current and temperature[20] as well as the current-induced effects on the pair breaking frequency[21] and depairing[22] In this work, we use the nonlinear kinetic inductance to controllably tune the resonant frequencies of LC resonators.

We have previously demonstrated the frequency tunability of superconducting microresonators designed to be particularly sensitive to the current-induced nonlinear kinetic inductance.[23] A distinctive feature of the first generation of devices was their aluminum wirebond-patched gap in the microstrip feedline, which functions as a temperature-controlled normal/superconducting switch (NSSW). When the temperature was above the critical temperature of aluminum ($T > T_c = 1.2$ K), the switch is in its normal state, redirecting the current into a narrow NbTiN strip inductor which dominates the total inductance of the LC resonator. This current flow modulates the kinetic inductance according to Eq. (1), thereby shifting the resonant frequency. Conversely, when $T < T_c$, the switch becomes superconducting, preventing any subsequent frequency shifts by shunting the current through the switch rather than allowing it to flow through the strip inductor.

Recently, we have further expanded on these tunable resonator devices with the kinetic inductance current sensor (KICS),[19] where we have introduced a new persistent current self-bias scheme. This approach enables us to adjust the bias and set the frequency shift above the $T_c$ of the NSSW. As the temperature is lowered below the $T_c$, the NSSW transitions from the normal to superconducting state, forming a superconducting current loop [illustrated as the red current loop in Fig. 1(c)]. According to the well-known principle of magnetic flux conservation, when the external bias current $I_b$ is removed, a persistent current $I_p \approx I_b$ continues to circulate within the loop and the frequency shift is locked. This persistent current technique has been utilized in other types of superconducting circuits, such as those used to flux bias metallic magnetic calorimeters (MMCs).[24]

The tunable resonator design implementing the NSSW and persistent current biasing scheme allows us to tune and lock the resonance frequency of a single resonator, which was demonstrated in the KICS work.[19] Instead of Al wirebonds which all have the same $T_c$, in this work we directly fabricated NSSWs on the wafer with variable $T_c$. This extends the persistent current biasing scheme to multiple resonators by making the NSSW of each resonator individually addressable. With

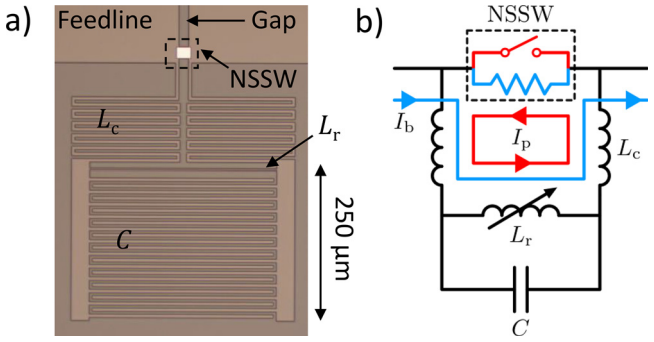


**FIG. 1.** Self-biased tunable resonator design incorporating a normal-superconducting switch (NSSW) and persistent current loop configuration. (a) Optical micrograph showing the resonator structure, including the feedline, NSSW, coupling inductor ($L_c$), nonlinear inductor ($L_r$), and interdigitated capacitor ($C$). (b) Circuit schematic illustrating the current paths in the device: external bias current path (blue) used for frequency tuning and the persistent current loop (red) that maintains the frequency shift after tuning. The NSSW functions as a temperature-controlled switch to direct current between these two paths.

addressable NSSWs, we can apply a desired bias current to the common feedline, "open" the NSSW by turning it normal, and then "close" the NSSW by turning it superconducting, locking the current and frequency of a target resonator. This procedure can be sequentially applied to each resonator until all resonances are properly adjusted and frequency collisions are resolved.

Our solution to achieve individually addressable devices is to fabricate resonator NSSWs with unique values of $T_c$ by exploiting the proximity effect.[25] We developed a special film deposition process, which is described below and illustrated in Fig. 2. First, we sputter a uniform 5 nm thick NbTiN film onto a high-resistivity Si wafer (see Ref. 26 for detailed deposition conditions). Without breaking vacuum, we then deposit an Al film on top of the NbTiN film while moving a custom-made shutter from left to right [see Fig. 2(a)]. This creates a thickness gradient in the Al film, varying from 250 nm at the wafer's left edge to 50 nm at its right edge. Following the deposition, we selectively etch the top Al layer, leaving a small patch only on the NSSW [see Fig. 1(a)], and then pattern the exposed NbTiN layer to form the feedline and resonator body. Due to the proximity effect, the varying thickness ratio between Al and NbTiN in each NSSW patch results in distinct $T_c$ values, which enables the desired addressable NSSW scheme for multiple resonators. We included a center row of $T_c$ test structures (5 mm x 5 mm squares) on the wafer to measure the resulting $T_c$ distribution. We connected 5 test structures (equally distributed across the wafer diameter) in series and measured their total resistance using a standard 4-wire measurement method in an adiabatic demagnetization refrigerator (ADR). The result is shown in Fig. 2(b). In this plot, the total resistance curve clearly shows 5 steps suggesting that the $T_c$ values are distinct for each sample and range between 1.2 and 3.1 K, meeting our need for individually addressing the NSSWs through temperature control of the ADR.

As shown in Fig. 3(a), a small array of four tunable resonators of identical design were connected in series and packaged in a device box. The device box was cooled down in an ADR with a controllable temperature range from 100 mK to 3 K. We measured the $S_{21}$ forward transmission using a vector network analyzer (VNA) in a standard

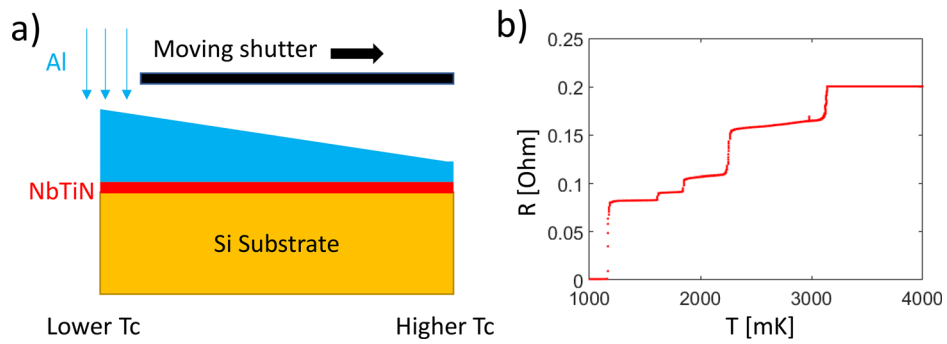


**FIG. 2.** Implementation of individually addressable normal-superconducting switches (NSSWs) using Al/NbTiN bilayer proximity effect. (a) Al/NbTiN bilayer deposition process utilizing a moving shutter. A thickness gradient in the top Al layer is created which results in a $T_c$ gradient across the wafer. (b) Total resistance measured from a series connection of 5 DC samples along the direction of the $T_c$ gradient. The different switches have different bilayer compositions, as the Al becomes thinner the Tc increases as well as the normal state resistance.

resonator measurement configuration [Fig. 3(b)]. The input line contained 40 dB of total attenuation, and the output line used a high-electron mobility transistor (HEMT) amplifier at the 4 K stage. A pair of bias tees was used to couple DC into the RF transmission line and provide the DC bias to the resonators. The four tunable resonator devices were selected across the wafer along the Al thickness gradient direction. Based on the measurements of nearby test structures, the $T_c$ values of these four resonators were expected to fall within the range of 1.9–2.5 K. This $T_c$ range was chosen for the convenience of temperature control using the ADR magnet.

The initial experiment aimed to determine the unique $T_c$ values of the NSSWs in the array. Without applying any bias current, we first cooled down the array to 1.9 K, ensuring the temperature was below the $T_c$ of each NSSW. The $S_{21}$ measurements, shown in Fig. 4(a), revealed that without DC bias, two of the four resonators exhibited frequency collision, which was not unexpected as the resonators share an identical geometry. After settling at 1.9 K, we applied a DC bias current of $I_b = 0.1$ mA through the bias tees. Since all NSSWs were in their superconducting state and effectively "closed" (zero resistance), the current bypassed the inductors of the resonators. Consequently, the resonant frequencies and $S_{21}$ remained unchanged. Next, we slowly ramped the bath temperature up from 1.9 to 2.5 K. When the temperature crosses the $T_c$ of an individual resonator's NSSW, the switch

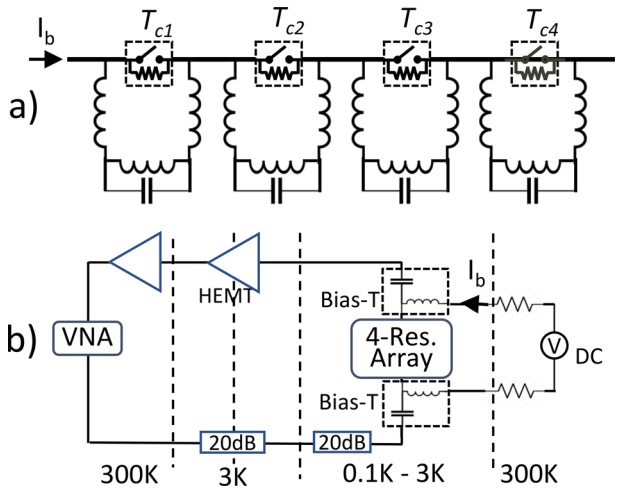


**FIG. 3.** Experimental setup. (a) A schematic diagram showing four self-biased tunable resonators selected from different parts of the wafer connected in series. The resonators are identical in design geometry except that their NSSW Al/NbTiN bilayer patches have different thicknesses and $T_c$. (b) A diagram showing the RF measurement chain. A DC bias current is generated by a constant voltage source in series with two 10 kΩ bias resonators and injected into the 4-resonator array through a pair of bias tees.

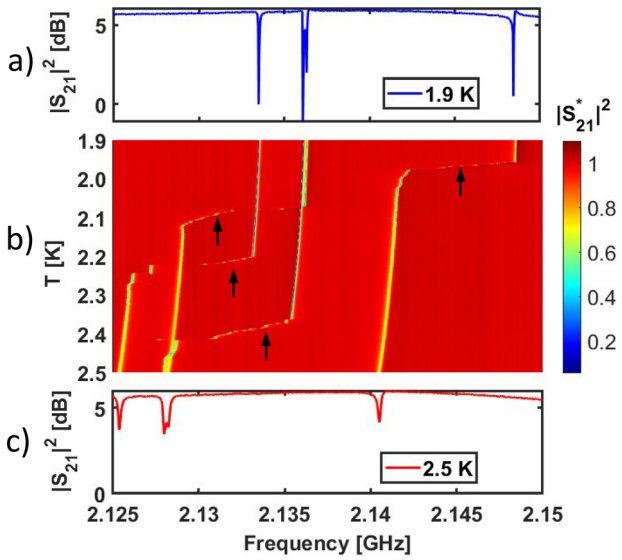


**FIG. 4.** Calibration of the critical temperatures of NSSWs by performing a temperature sweep from 1.9 to 2.5 K while applying a constant bias current of $I_b = 0.1$ mA. (a) Initial $|S_{21}|^2$ measured at 1.9 K before the temperature ramp-up. (b) Color-coded $|S^*_{21}|^2$ magnitude plot showing the resonator frequency trajectories during the ramp-up. The data are normalized by the background transmission measured with all resonances tuned out of range (by applying current). All resonant frequencies shift down gradually with temperature due to the temperature dependence of thermal quasiparticle density. A step change in the trajectory along the frequency axis occurs as the bath temperature crosses the $T_c$ of a given resonator's NSSW (black arrows). (c) Final $|S_{21}|^2$ measured at $T = 2.5$ K after the temperature ramp-up.

transitions to its normal state and is effectively "open," forcing the current into the inductor and shifting the resonant frequency of the corresponding resonator. Figure 4(b) shows the resonant frequency trajectories of the four resonators during the temperature ramp-up process. We observed distinct downward frequency shifts (indicated by black arrows) at the critical temperatures $T_{c_1} = 2.39$ K, $T_{c_2} = 2.22$ K, $T_{c_3} = 2.10$ K, and $T_{c_4} = 1.97$ K (here we denote the resonators 1–4 in descending order of their $T_c$ values), demonstrating the successful identification of each NSSW's unique $T_c$. At the final temperature of 2.5 K, all the resonators are shifted by the same amount and the frequency collision remains, as shown in Fig. 4(c). Moreover, based on the trajectory analysis, we have identified that the frequency collision feature occurring at $\sim 2.136$ GHz originates from resonators 1 and 3.

Following the $T_c$ calibration, we perform calibration of the relationship between resonant frequency shift and bias current. This calibration will be utilized later for fine-tuning the resonant frequencies. The measurement was performed at $T = 2.5$ K where the NSSWs of all four resonators were in the normal state, and the bias current flowed through each resonator inductor. Figure 5 shows the measured fractional frequency shift $\delta f_r/f_r$ plotted as a function of $I_b$. Only resonators 2 and 4 were measured due to the frequency collision between resonators 1 and 3. We see from Fig. 5 that $\delta f_r/f_r$ has a quadratic dependence on $I_b$. The curves for resonators 1 and 3 are almost overlapping, which suggests that we may use the fitted curve as the "standard" curve to tune all the 4 resonators. Figure 5 also shows that the frequency tuning range is limited to $|\delta f_r/f_r| = 3.5\%$ at a bias current of $I_b = 0.32$ mA. The effect of the bias current on the resonator loss was studied earlier, for frequency shifts of 3%, the extra internal loss was measured to be less than $10^{-6}$,[23] and in other similar KICS structures[19] frequency shifts of 15% have been observed. The best KICS signal to noise performance was found at roughly 75% of the maximum bias, at the highest currents additional nonlinear effects begin to turn on and the devices are less stable.[19]

As the first *in situ* frequency tuning experiment, we demonstrate moving all four resonators to a single frequency. Since the current-induced kinetic inductance (Eqn. 1) only allows downward frequency tuning, we chose the lowest resonant frequency (resonator 2) as the common frequency target, as shown by the tuning plan in Fig. 6(a). We continuously monitored resonant frequencies using a VNA over a

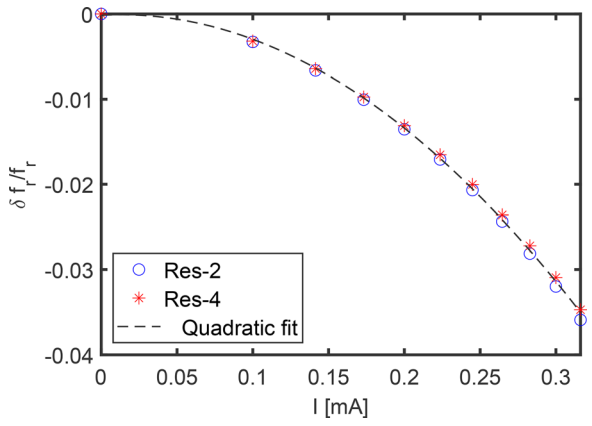


**FIG. 5.** Fractional frequency shift $\delta f_r/f_r$ of resonators 2 and 4 vs $I_b$ measured at $T = 2.5$ K. The dashed line shows a quadratic fit $\delta f_r/f_r = 1/2(I/I^*)^2$ to the data. From the fit, we extrapolate $I^* = 1.1$ mA.

frequency range of 2.128–2.147 GHz while simultaneously recording the sample stage temperature. For this experiment, the bias current and sample stage temperature were manually controlled. The results of this tuning process are shown in Fig. 6(b). Starting from an initial state of $T = 2.5$ K and $I_b = 0$ [top panel, Fig. 6(b)], we sequentially tuned and locked individual resonators. For each target resonator, we first maintain the temperature above its NSSW $T_c$ while manually adjusting the bias current until its resonant frequency shifted down to match the desired target frequency. The sample stage was then cooled to a temperature below the target resonator's NSSW $T_c$ but above the $T_c$ of the subsequent target resonator's NSSW. During the cooling process, the desired persistent current in the target resonator was established and the desired resonant frequency of the target resonator was permanently locked. This two-step tuning/locking procedure was repeated for all four resonators, concluding at $T = 1.9$ K with all frequencies successfully locked. The bias current was then removed without disturbing the locked frequencies. The right panel displays the temperature evolution over time, where blue regions indicate current tuning steps (at constant temperature) and pink regions indicate frequency locking steps (temperature cooling). The middle panel of Fig. 6(b) shows a color-coded plot of $S_{21}$ vs time, with resonant frequencies appearing as bright trajectories. We see that during frequency tuning steps, multiple resonator frequency trajectories shift simultaneously, while only one trajectory remains fixed after each subsequent frequency locking step. To better illustrate the process, Fig. 6(c) shows the current flow configuration at each step of the current and frequency adjustment sequence. Since the quantization of magnetic flux implies that the persistent bias currents in the locked state are also quantized, the frequency resolution is finite. However, due to the large loop area visible in Fig. 1 and the mA scale bias currents, the magnetic flux in the loop is many times the flux quantum and we are not able to resolve any discrete frequency placement. The final state, shown in the bottom panel of Fig. 6(b), clearly reveals four overlapping resonances, successfully demonstrating the *in situ* frequency tuning and locking procedure. Further investigation into the limits of the frequency resolution are ongoing.

For the second demonstration, we aim to tune the four resonators into an evenly spaced frequency comb configuration while correcting the initial frequency collision. This goal can be accomplished by tuning resonators 1 and 2 to lower frequencies while keeping the resonant frequencies of resonators 3 and 4 constant, as shown in Fig. 7(a). Building upon our experience during the first demonstration, we developed an automated procedure to set the bias current (via the voltage source) and control the ADR temperature (via the ADR magnet). The auto-tuning protocol executes a sequence of current adjustments along the cooling path from 2.5 to 1.9 K: $I_b$ was set to 0.041 mA at 2.51 K, 0 mA at 2.3 K, 0 mA at 2.15 K, 0.123 mA at 2.04 K, and 0 mA at 1.9 K. These current values were derived from the desired frequency shifts and from the measured relationship between $\delta f_r/f_r$ and $I_b$ at 2.5 K (Fig. 5). Figure 7(b) shows $S_{21}$ measured before (blue) and after (red) the current adjustment at each temperature step. The final state, shown in the bottom panel of Fig. 7(b), clearly reveals four nearly evenly spaced resonance peaks, demonstrating successful *in situ* frequency tuning and locking of the resonator array to a collision-free frequency comb. Resonators biased at these low persistent currents are stable for the length of an ADR hold time, i.e., several days, but stability investigations on longer timescales continue.

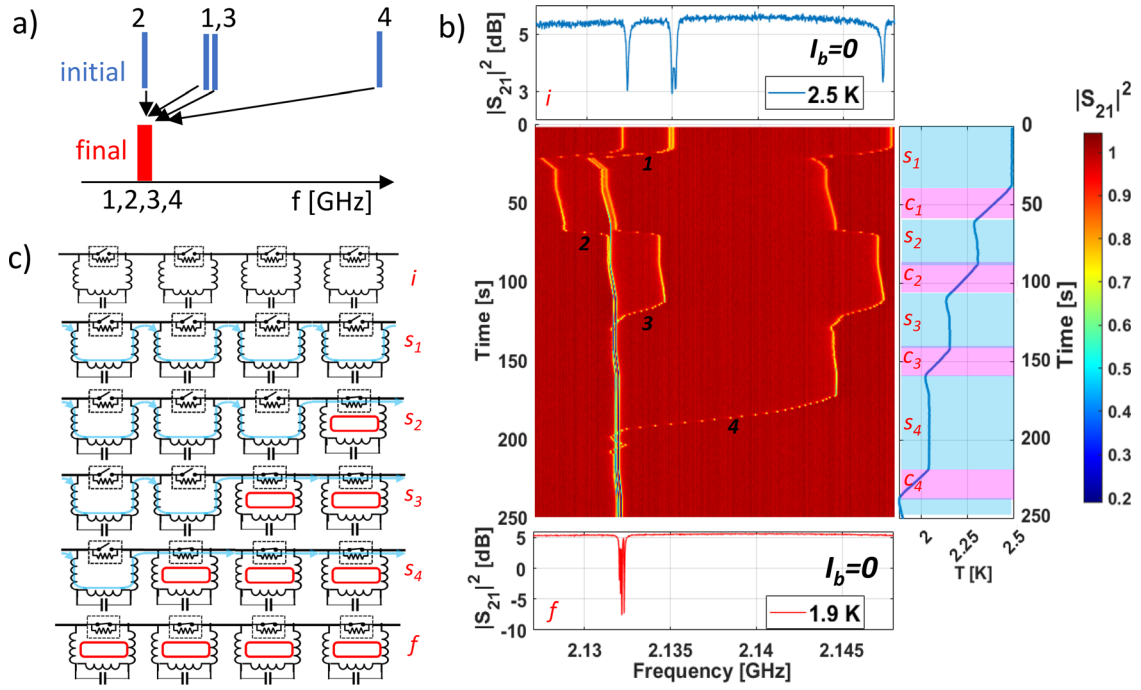


**FIG. 6.** Demonstration of tuning and locking multiple resonators to an identical frequency. (a) Schematic showing the frequency tuning plan, with arrows indicating the intended frequency shifts for each resonator. (b) Time evolution of the tuning process shown through four panels: the top panel shows initial (with label "i") $S_{21}$ measurement at $T = 2.5$ K; the middle panel displays color-coded normalized $|S_{21}^*|^2$ magnitude over time, with bright trajectories indicating resonant frequencies; the bottom panel shows final (with label "f") $S_{21}$ measurement at $T = 1.9$ K; the right panel shows temperature evolution with blue regions indicating current tuning steps (with labels "$s_1$" to"$s_4$") and pink regions indicating frequency locking steps (with labels "$c_1$" to"$c_4$"). (c) Schematic diagrams showing NSSW status and current flow configurations during each tuning step (corresponding to the blue regions in the temperature plot). External bias current paths are shown in blue and persistent current loops are shown in red.

We presented an improved *in situ* frequency tuning technique that leverages nonlinear kinetic inductance and persistent current in superconducting loops. The method uses temperature-controlled normal/superconducting switches with distinct critical temperatures to individually address and tune resonators during device cooldown. Two key demonstrations were achieved: tuning multiple resonators to a single common frequency and creating an evenly spaced frequency comb while resolving initial frequency collisions. While our initial proof-of-concept demonstration used a modest four-resonator array, this method shows promise for scaling. Using the available temperature

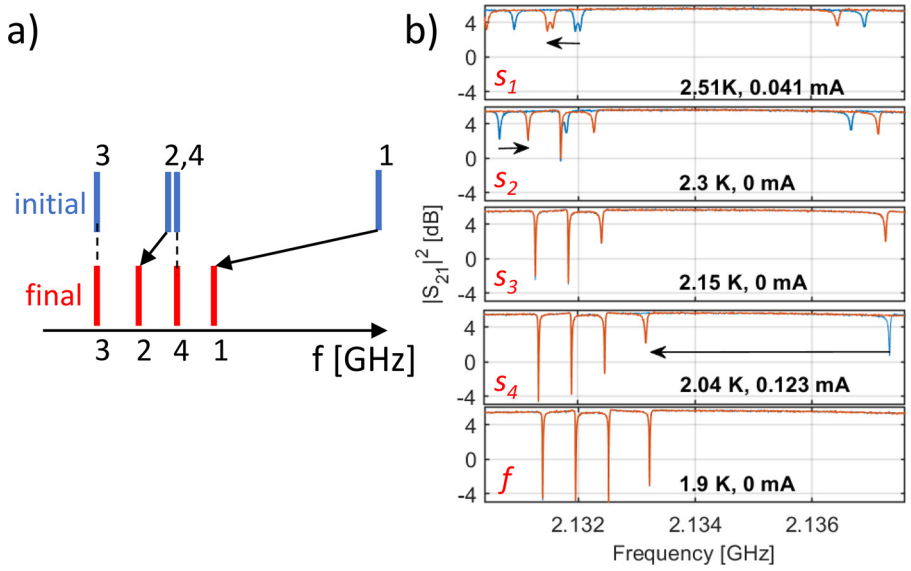


**FIG. 7.** Automated frequency tuning-locking demonstration creating an evenly spaced frequency comb. (a) Schematic showing the frequency tuning plan, with arrows indicating the intended frequency shifts to resolve the initial frequency collision between resonators 2 and 4 while creating uniform frequency spacing. (b) $S_{21}$ measurements at different temperature way-points during the automated tuning process, with blue traces showing measurements before current adjustment and red traces showing measurements after current adjustment. The final state (bottom panel) demonstrates successful correction of the frequency collision and establishment of a well-spaced frequency comb.

window between the transition temperatures of NbTiN ($T_c = 13$ K) and Al ($T_c = 1.2$ K), and assuming a transition width of 50 mK per NSSW, we project the capability to independently tune more than 200 resonators on a single bias line. Resonators with closer $T_c$ switch spacing will quantify how many resonators can be independently tuned. Scaling to even larger arrays can be achieved by implementing N independent current bias lines to control N distinct sub-arrays. Additionally, we are investigating alternative NSSW control mechanisms, such as flux biasing and optical activation, to further enhance the scalability and functionality. The technique was successfully automated using computer-controlled procedures, providing a universal solution for improving yield and multiplexing density in large resonator arrays without requiring post-fabrication processing. This advancement is particularly important for scaling up superconducting detector and qubit systems where precise frequency control and reduced crosstalk are critical.

This material is based upon work supported by NASA (Award Nos. NNH23OB118A and 80NSSC25K7636). The authors would like to thank Raymond Simmonds and Avirup Roy for helpful discussions on the manuscript.

## AUTHOR DECLARATIONS

### Conflict of Interest

The authors have no conflicts to disclose.

### Author Contributions

**M. R. Vissers:** Conceptualization (equal); Formal analysis (equal); Investigation (equal); Writing – original draft (equal); Writing – review & editing (equal). **J. D. Wheeler:** Formal analysis (equal); Investigation (equal); Writing – original draft (equal); Writing – review & editing (equal). **P. Szypryt:** Formal analysis (equal); Investigation (equal); Writing – original draft (equal); Writing – review & editing (equal). **A. Giachero:** Formal analysis (equal); Writing – original draft (equal); Writing – review & editing (equal). **J. E. Austermann:** Formal analysis (equal); Writing – original draft (equal); Writing – review & editing (equal). **J. Hubmayr:** Formal analysis (equal); Writing – original draft (equal); Writing – review & editing (equal). **G. C. O'Neil:** Conceptualization (equal); Formal analysis (equal); Investigation (equal); Writing – original draft (equal); Writing – review & editing (equal). **J. N. Ullom:** Supervision (equal); Writing – original draft (equal); Writing – review & editing (equal). **J. Gao:** Conceptualization (equal); Formal analysis (equal); Investigation (equal); Software (equal); Supervision (equal); Writing – original draft (equal); Writing – review & editing (equal).

## DATA AVAILABILITY

The data that support the findings of this study are available from the corresponding author upon reasonable request.

## REFERENCES

[1]A. Blais, R.-S. Huang, A. Wallraff, S. M. Girvin, and R. J. Schoelkopf, Phys. Rev. A **69**, 062320 (2004).
[2]A. Wallraff, D. I. Schuster, A. Blais, L. Frunzio, R.-S. Huang, J. Majer, S. Kumar, S. M. Girvin, and R. J. Schoelkopf, Nature **431**, 162 (2004).
[3]P. K. Day, H. G. LeDuc, B. A. Mazin, A. Vayonakis, and J. Zmuidzinas, Nature **425**, 817 (2003).
[4]J. Mates, G. C. Hilton, K. D. Irwin, L. R. Vale, and K. Lehnert, Appl. Phys. Lett. **92**, 023514 (2008).
[5]P. Szypryt, S. R. Meeker, G. Coiffard, N. Fruitwala, B. Bumble, G. Ulbricht, A. B. Walter, M. Daal, C. Bockstiegel, G. Collura *et al.*, Opt. Express **25**, 25894 (2017).
[6]J. Wheeler, J. Austermann, M. Vissers, J. Beall, J. Gao, J. Imrek, E. Heilweil, D. Bennett, J. Gard, J. van Lanen *et al.*, Proc. SPIE **12190**, 1219006 (2022).
[7]H. McCarrick, E. Healy, Z. Ahmed, K. Arnold, Z. Atkins, J. E. Austermann, T. Bhandarkar, J. A. Beall, S. M. Bruno, S. K. Choi *et al.*, Astrophys. J. **922**, 38–4357 (2021).
[8]X. Liu, W. Guo, Y. Wang, L. Wei, C. Mckenney, B. Dober, T. Billings, J. Hubmayr, L. Ferreira, M. Vissers *et al.*, J. Appl. Phys. **122**, 034502 (2017).
[9]X. Liu, W. Guo, Y. Wang, M. Dai, L. F. Wei, B. Dober, C. M. McKenney, G. C. Hilton, J. Hubmayr, J. E. Austermann *et al.*, Appl. Phys. Lett. **111**, 252601 (2017).
[10]R. Parmenter, *Nonlinear Electrodynamics of Super-Conductors With a Very Small Coherence Distance* (RCA (Radio Corporation of America) Review (US), 1962), p. 23.
[11]J. Zmuidzinas, Annu. Rev. Condens. Matter Phys. **3**, 169 (2012).
[12]B. Ho Eom, P. K. Day, H. G. Leduc, and J. Zmuidzinas, Nat. Phys. **8**, 623 (2012).
[13]M. Malnou, M. Vissers, J. Wheeler, J. Aumentado, J. Hubmayr, J. Ullom, and J. Gao, PRX Quantum **2**, 010302 (2021).
[14]A. Giachero, M. Vissers, J. Wheeler, L. Howe, J. Gao, J. Austermann, J. Hubmayr, A. Nuc-ciotti, and J. Ullom, J. Low Temp. Phys. **215**, 152 (2024).
[15]D. Cunnane, H. G. Leduc, N. Klimovich, F. Faramarzi, A. Beyer, and P. Day, Appl. Phys. Lett. **124**, 022601 (2024).
[16]G. Giesbrecht, N. E. Flowers-Jacobs, A. Sirois, M. A. Castellanos-Beltran, M. Vissers, J. Gao, T. Barton, and P. Dresselhaus, IEEE Trans. Appl. Supercond. **35**, 1 (2025).
[17]A. Kher, P. K. Day, B. H. Eom, J. Zmuidzinas, and H. G. Leduc, J. Low Temp. Phys. **184**, 480 (2016).
[18]S. Sypkens, L. Minutolo, S. Patel, E. Knehr, A. B. Walter, H. G. Leduc, L. Narváaez, R. Cham- berlin, T. Jamison-Hooks, M. D. Shaw *et al.*, Appl. Phys. Lett. **124**, 262602 (2024).
[19]P. Szypryt, D. A. Bennett, I. Fogarty Florang, J. W. Fowler, A. Giachero, R. Hummatov, A. E. Lita, J. A. Mates, S. W. Nam, G. C. O'Neil *et al.*, Commun. Eng. **3**, 160 (2024).
[20]A. J. Annunziata, D. F. Santavicca, L. Frunzio, G. Catelani, M. J. Rooks, A. Frydman, and D. E. Prober, Nanotechnology **21**, 445202 (2010).
[21]S. Zhao, S. Withington, D. J. Goldie, and C. N. Thomas, J. Phys. D **53**, 345301 (2020).
[22]J. R. Clem and V. Kogan, Phys. Rev. B—Condens. Matter Mater. Phys. **86**, 174521 (2012).
[23]M. R. Vissers, J. Hubmayr, M. Sandberg, S. Chaudhuri, C. Bockstiegel, and J. Gao, Appl. Phys. Lett. **107**, 062601 (2015).
[24]A. Fleischmann, C. Enss, and G. Seidel, *Metallic Magnetic Calorimeters* (Springer, Berlin, Heidelberg, 2005), pp. 151–216.
[25]N. R. Werthamer, Phys. Rev. **132**, 2440 (1963).
[26]A. Giachero, M. Vissers, J. Wheeler, M. Malnou, J. Austermann, J. Hubmayr, A. Nucciotti, J. Ullom, and J. Gao, IEEE Trans. Appl. Supercond. **33**, 1 (2023).